Mono-Substituted Isopropylated Triaryl Phosphate, a Major Component of Firemaster 550, is an AHR Agonist that Exhibits AHR-Independent Cardiotoxicity in Zebrafish

Cory V. Gerlach[*], **Siba R. Das**[*], **David C. Volz**[†], **William H. Bisson**[*], **Siva K. Kolluri**[*], and **Robert L. Tanguay**[*,1]

[*]Department of Environmental and Molecular Toxicology, Oregon State University, Corvallis, Oregon USA

[†]Department of Environmental Health Sciences, Arnold School of Public Health, University of South Carolina, Columbia, South Carolina USA

Abstract

Firemaster 550 (FM550) is an additive flame retardant mixture used within polyurethane foam and is increasingly found in house dust and the environment due to leaching. Despite the widespread use of FM550, very few studies have investigated the potential toxicity of its ingredients during early vertebrate development. In the current study, we sought to specifically investigate mono-substituted isopropylated triaryl phosphate (mITP), a component comprising approximately 32% of FM550, which has been shown to cause cardiotoxicity during zebrafish embryogenesis. Previous research showed that developmental defects are rescued using an aryl hydrocarbon receptor (AHR) antagonist (CH223191), suggesting that mITP-induced toxicity was AHR-dependent. As zebrafish have three known AHR isoforms, we used a functional AHR2 knockout line along with AHR1A-and AHR1B-specific morpholinos to determine which AHR isoform, if any, mediates mITP-induced cardiotoxicity. As *in silico* structural homology modeling predicted that mITP may bind favorably to both AHR2 and AHR1B isoforms, we evaluated AHR involvement *in vivo* by measuring CYP1A mRNA and protein expression following exposure to mITP in the presence or absence of CH223191 or AHR-specific morpholinos. Based on these studies, we found that mITP interacts with both AHR2 and AHR1B isoforms to induce CYP1A expression. However, while CH223191 blocked mITP-induced CYP1A induction and cardiotoxicity, knockdown of all three AHR isoforms failed to block mITP-induced cardiotoxicity in the absence of detectable CYP1A induction. Overall, these results suggest that, while mITP is

[1]To whom correspondence should be addressed: Department of Environmental and Molecular Toxicology, Sinnhuber Aquatic Research Laboratory, Oregon State University, 28645 East Highway 34, Corvallis, OR 97333. Fax: (541) 737-6074. Robert.Tanguay@oregonstate.edu.

Supplementary Data: Results from mITP concentration-response and CH223191 co-exposures studies are provided within Supplementary File 1.

an AHR agonist, mITP causes AHR-independent cardiotoxicity through a pathway that is also antagonized by CH223191.

Keywords

aryl hydrocarbon receptor (AHR); cardiotoxicity; Firemaster 550; flame retardant; zebrafish; CH223191

1. Introduction

In 2004, the commercial polybrominated diphenyl ether (PBDE) mixture known as PentaBDE – a widely used brominated flame retardant (FR) – was voluntarily phased out in the United States due to concerns about persistence, bioaccumulation, and toxicity (Rahman *et al.*, 2001; Tullo, 2003). As a result of strict fire safety standards set for low-density polyurethane foam in residential furniture and baby products, brominated and aryl phosphate ester (APE) components of the replacement FR mixture formulation known as Firemaster 550 (FM550) have been detected at concentrations comparable to and, in some cases, higher than total PBDE concentrations in household dust (Meeker and Stapleton, 2010; Springer *et al.*, 2012; Stapleton *et al.*, 2008; Stapleton *et al.* 2009). Moreover, brominated components of FM550 have been found in municipal sewage (Davis *et al.*, 2012), urban and rural air samples (Ma *et al.*, 2012), and marine mammal tissue (Lam *et al.*, 2009). The high detection of FM550 components suggests that chronic human exposure following migration from treated end-use products is common within the US. Therefore, similar to concerns about PBDEs (Costa and Giordano, 2007; Herbstman *et al.*, 2010), a better understanding of the potential effects of prenatal FM550 exposure resulting from maternal ingestion of contaminated house dust is needed since these stages may be more susceptible relative to later periods of development.

Using zebrafish (*Danio rerio)* as a model, McGee *et al.* (2013) recently evaluated the potential developmental toxicity of brominated and APE components present within FM550. The brominated component of FM550 consists of 2-ethylhexyl-2,3,4,5-tetrabromobenzoate (TBB, ~30%) and bis (2-ethylhexyl) tetrabromophthalate (TBPH, ~8%), whereas the APE component (~62%) consists of triphenyl phosphate (TPP, ~17%) and isopropylated triaryl phosphates (ITPs, ~45%) (McGee *et al.*, 2013). The ITP component is a complex mixture of ortho-, meta-, and para-substituted isomers of mono-, di-, tri-, and tetra-ITPs comprising approximately 32%, 10%, 2.4%, and 0.4% of FM550, respectively (McGee *et al.*, 2013). Within their study, McGee *et al.* (2013) demonstrated that exposure to TPP and mono-ITP (mITP) – but not TBB, TBPH, di-ITP, nor tri-ITP – resulted in severe pericardial edema (PE) and blocked normal looping of the atrium and ventricle, resulting in a "tube heart" phenotype.

Using an aryl hydrocarbon receptor (AHR) antagonist (CH223191), McGee *et al.* (2013) reported that mITP-induced – but not TPP-induced – cardiac abnormalities and cytochrome P450 1A (CYP1A) expression within zebrafish embryos were aryl hydrocarbon receptor (AHR)-dependent. While mammals have only one AHR, zebrafish have three AHR isoforms: AHR1A, AHR1B, and AHR2 (Andreasen *et al.*, 2002; Karchner *et al.*, 2005;

Tanguay *et al.*, 1999). AHR2 is the functional AHR paralog in zebrafish that mediates toxicity for 2,3,7,8-tetrachlorodibenzo-*p*-dioxin (TCDD) (Prasch *et al.*, 2003), 3,3′,4,4′,5-pentachlorobiphenyl (PCB126) (Jönsson *et al.*, 2012), and many polycyclic aromatic hydrocarbons (PAHs) (Incardona *et al.*, 2006). Although the functionalities of AHR1B and AHR1A are not well characterized, emerging evidence suggests that some PAH mixtures, PCB126, and the non-classical AHR agonist leflunomide can activate AHR1A and/or AHR1B, induce CYP1A expression, and mediate developmental toxicity (Garner *et al.*, 2013; Goodale *et al.*, 2012; Incardona *et al.*, 2006; Incardona *et al.*, 2011). Therefore, McGee *et al.* (2013) began investigating the AHR-isoform dependence of mITP in zebrafish using an AHR2-specific translation-blocking morpholino (MO). However, AHR2 knockdown failed to block mITP-induced cardiac abnormalities, suggesting that this phenotype was mediated through an AHR2-independent pathway.

As mITP-induced cardiotoxicity and CYP1A induction were blocked by CH223191 but not AHR2 knockdown, one of the key questions arising from this study was whether cardiotoxicity is mediated by an AHR1A and/or AHR1B-dependent pathway. Therefore, we first used *in silico* structural modeling – an approach previously used to predict AHR ligand binding (Bisson *et al.*, 2009; Goodale *et al.*, 2012) – to determine whether mITP would dock favorably with the AHR2, AHR1A, and AHR1B ligand-binding domains (LBDs). *In vivo* studies using zebrafish were then conducted to determine whether AHR1A and/or AHR1B contribute to mITP-induced cardiotoxicity during early embryonic development. In order to eliminate the potential for incomplete AHR2 knockdown with transient MOs, and to better investigate the individual roles of AHR1A and AHR1B isoforms, a functional zebrafish AHR2 knockout line was utilized.

2. Materials and Methods

2.1. Chemicals

mITP (90%) (Figure 1) was originally provided as FM550 (Chemtura) via Dr. Susan Klosterhaus (Cradle to Cradle Products Innovation Institute, San Francisco, CA) and was purified by Wellington Laboratories (Guelph, Ontario, Canada) as previously described (McGee *et al.*, 2013). Due to the lack of commercially available analytical standards for mITPs, exact ratios of mITP congeners (*ortho*, *meta*, *para*) within our mITP fraction are unknown. The AHR antagonist, 2-methyl-2H-pyrazole-3-carboxylic acid (2-methyl-4-o-tolylazo-phenyl)-amide (CH223191, >99%) (Figure 1), was purchased from Tocris Bioscience (Ellisville, MO). All stock solutions were dissolved in ACS-grade dimethyl sulfoxide (DMSO).

2.2. Zebrafish lines and embryos

All adult zebrafish were housed in accordance to approved Institutional Animal Care and Use Committee (IACUC) protocols at Oregon State University on a recirculating water system at $28\pm1°C$ with a 14-hour light/10-hour dark schedule. Embryos from adult 5D zebrafish were obtained from group spawns as previously described (Reimers *et al.*, 2006). All *ahr2*[hu3335] embryos were obtained from gated crosses with ∼1:1 ratio of male to female. All embryos were collected within one-hour post fertilization (hpf), rinsed, and kept in petri

dishes with E2 embryo medium at 28±1°C until treatment. The *ahr2*[hu3335] line were mutagenized via Targeting Induced Local Lesions IN Genomes as previously described (Goodale *et al.*, 2012).

2.3. Molecular modelling and docking

Homology models of human AHR (hAHR), and zebrafish AHR2, AHR1A, and AHR1B LBDs in the *apo* conformation were initially built as previously reported (Bisson *et al.*, 2009; Goodale *et al.*, 2012). TCDD, CH223191, and *ortho*, *meta*, and *para* mITP congeners were docked into hAHR, zebrafish AHR2, AHR1A, and AHR1B. *In vivo* studies have shown TCDD is a strong agonist for only AHR2 and AHR1B (Andreasen *et al.*, 2002; Goodale *et al.*, 2012; Karchner *et al.*, 2005). The co-bound models were then submitted to 10^5 steps ligand-protein side chain optimization through Monte Carlo (MC) simulations in the internal coordinate space with Molsoft ICM (Katritch *et al.*, 2012; manuscript submitted). The highest rank energy complex obtained from each simulation was used for molecular docking. Both tautomerization states (HisD and HisE) of human residue His 291 and zebrafish AHR2 and AHR1B His 296 homologues were considered.

Each receptor was represented by five types of interaction potentials: (i) van der Waals potential for a hydrogen atom probe; (ii) van der Waals potential for a heavy-atom probe (generic carbon of 1.7 Å radius); (iii) optimized electrostatic term; (iv) hydrophobic terms; and (v) lone-pair-based potential, which reflects directional preferences in hydrogen bonding. The energy terms were based on the Merck Molecular Force Field (MMRF) to account for solvation free energy and entropic contribution (Totrov and Abagyan, 2001). Modified intermolecular terms such as soft van der Waals, hydrogen bonding, and hydrophobicity were added. Conformational sampling was based on the biased probability Monte Carlo (BPMC) procedure, which randomly selects a conformation in the internal coordinate space and then initiates a step to a new random position independent of the previous one – but according to a predefined continuous probability distribution – since, after each random step, full local minimization greatly improves the efficiency of the procedure. In the ICM-VLS (Molsoft ICM) screening procedure, the ligand scoring was optimized to obtain maximal separation between binders and non-binders. Based on fit within the receptor, each compound was assigned an ICM score that accounts for continuum and discreet electrostatics as well as hydrophobicity and entropy parameters (Totrov and Abagyan, 2001; Abagyan *et al.*, 1994).

2.4. mITP exposures and developmental toxicity assessments

mITP exposures were conducted using a static exposure protocol. Embryos were batch-exposed with chorions intact in 20-mL glass vials. Vials were prewashed with Liquinox® and hot water, and then RO-rinsed. Vials were loaded with 10 viable embryos (6-to-8 hpf) using polished glass pipettes, and 7 mL of mITP or vehicle control (0.1% DMSO) in E2 embryo medium was added. Each treatment group consisted of three replicate vials that were incubated at 28±1°C with a 14-hour light/10-hour dark schedule until 72 hpf for qPCR and immunohistochemistry experiments and 120 hpf for concentration-response and CH22391 studies.

Preliminary range-finding studies were conducted at intervals between 0.1 and 1.6 μM mITP, monitored daily, and screened closely for malformations at 120 hpf. Necrotic embryos were removed daily. Based on these range-finding studies, the 0.2 μM mITP concentration was selected for the remaining experiments because it was the lowest concentration where PE was easily discernable, CYP1A induction was strong, and CYP1A induction was rescued with AHR knockdown. At 120 hpf, fish were evaluated for absence or presence of PE and euthanized via prolonged immersion within an overdose of tricaine methanesulfonate (MS-222).

2.5. CH223191 co-exposures

We first used CH223191 – an AHR antagonist (Kim *et al.* 2006) – to replicate findings reported within McGee *et al.* (2013). Based on initial range-finding studies, as well as studies in McGee *et al.* (2013), 0.5 μM CH223191 was used for all mITP co-exposure experiments. For mITP co-exposures experiments, groups of 50 5D embryos were pre-exposed to either 20 mL of 0.5 μM CH223191 or 0.1% DMSO in glass petri dishes from 0.75 to 6 hpf. At 6 hpf, 10 embryos per replicate (three replicate vials per treatment) were moved to 20 mL glass vials and treated with 7 mL of 0.1% DMSO or 0.2 μM mITP in the absence or presence of 0.5 μM CH223191 using a static exposure protocol. Vials were incubated at 28±1°C with a 14-hour light/10-hour dark schedule until 120 hpf. Necrotic embryos were removed daily. At 120 hpf, fish were evaluated for the absence or presence of PE and then euthanized with MS-222.

2.6. Morpholino injections

Fluorescein-tagged MO anti-sense oligonucleotides were designed against AHR1A and AHR1B zebrafish isoforms and purchased from Gene Tools (Philomath, OR). An AHR1A splice-blocking MO (AHR1A MO, 5′-CTTTTGAAGTGACTTTTGGCCCGCA-3′) (Incardona *et al.*, 2006) and an AHR1B splice-blocking MO (AHR1B MO, 5′-ACACAGTCGTCCATGATTACTTTGC-3′) (Goodale *et al.*, 2012) were used for all experiments. A standard control MO from Gene Tools (CoMO, 5′-CCTCTTACCTCAGTTACAATTTATA-9) was utilized as a negative control. All embryos were injected at the one-cell stage with approximately 2 nL of 0.75 mM MO dissolved in ultrapure water and 0.5% phenol red. All embryos were allowed to develop in E2 embryo medium post-injection until 5 hpf and then selected based on intensity and even distribution of fluorescence in blastomeres using an epifluorescent stereoscope.

2.7. Immunohistochemistry

Before performing immunohistochemistry (IHC), 72-hpf 5D and *ahr2*[hu3335] embryos were fixed in 4% paraformaldehyde overnight on a rocker at 4°C. Fixed embryos were then washed twice with phosphate-buffered saline with Tween® 20 (PBST) for 30 min, DI water for 1 hour, and placed in -20°C in acetone and ice for 20 min. Samples were then treated with collagenase (1 mg/mL within PBST) for 50 min, then washed twice with PBST for 30 min, and treated with 10% normal goat serum (NGS) for 1 hour. Samples were then treated with a Biosense mouse α fish CYP1A monoclonal primary antibody (1:500 dilution in 10% NGS) and incubated overnight at 4°C on a rocker. On day two, embryos were rinsed three

times in PBST for 30 min and treated with an Alexa Fluor 594 goat α mouse secondary antibody (1:1000 dilution in 10% NGS) for 2 hours on a rocker at room temperature. Embryos were rinsed three times with PBST before imaging. At least 8 embryos per replicate group (three replicate groups per treatment) were evaluated and representative images were captured using a Zeiss Axiovert 200 M epifluorescent microscope with 5X objective using a 1-s exposure time.

2.8. Total mRNA extraction and PCR

For all exposure scenarios utilizing 5D and *ahr2*[hu3335] lines at least nine 72-hpf embryos per replicate group (three replicate groups per treatment) were homogenized in 500 μL RNAzol and stored at -78°C. To extract total RNA for real-time qPCR studies, samples were thawed at room temperature and 200 μL of ultrapure water was added, shaken vigorously, and centrifuged at 12,000 rpm for 15 min. Supernatant was removed and 500 μL isopropanol was added, vortexed, and centrifuged at 12,000 rpm for 10 min. The resulting RNA pellet was then washed three times in 75% ethanol and centrifuged at 8,000 rpm for 3 min between washes. The pellet was dissolved in 20 μL water and total RNA concentration was measured using SynergyMx microplate reader (Biotek) with the Gen5 Take3 module. Total RNA was then diluted to 200 ng/μL, and single-strand cDNA was generated using a high-capacity cDNA Reverse Transcription kit (Applied Biosystems) with MultiScribe™ Reverse Transcriptase per manufacturer's instructions. All resulting cDNA was stored at -20°C until use.

Relative abundance of *cyp1a*, *ahr1a*, *ahr1b*, and *β-actin*, mRNA transcripts was measured for each exposure scenario using real-time qPCR. All primer sequences utilized in this study were previously used in Goodale *et al.* (2012) and are listed in Table 1. All realtime qPCR samples were performed in 20-μL reaction volumes containing 10 μL Power SYBR® Green PCR master mix (Applied Biosystems), 0.5 μL of each forward and reverse primer (each 5 μM), 4 μL ultrapure water, and 100 ng equivalents of cDNA (5 μL at 20 ng/μL cDNA). Amplification was performed with StepOnePlus™ (Applied Biosystems) using cycling conditions as follows: 50°C for 2 min; 95°C for 15 min; 40 cycles of 95°C for 10 s, 60°C for 20 s, and 72°C for 30 s. Real-time qPCR analysis was completed using StepOne Software v2.1 (Applied Biosystems) with the C_T method normalized to *β-actin*. All samples were analyzed using StatView 5.01 (SAS Institute, Inc.) and one-way ANOVA ($p < 0.05$). For confirmation of *ahr1a* and *ahr1b* knockdown, qualitative PCR was performed in 25-μL reaction volumes using Novagen® KOD Hot Start DNA Polymerase per manufacture's instructions, and PCR products were then separated on a 1.7% agarose gel containing ethidium bromide.

3. Results

3.1. mITP is predicted to bind AHR2 and AHR1B but not AHR1A

TCDD, CH223191 and the *ortho-*, *meta-* and *para-*mITP congeners were docked into hAHR and zebrafish AHR2, AHR1B and AHR1A models (Table 2). In hAHR, TCDD docked with a score of -24.11 (His 291-D) establishing a hydrogen bond (HB) with the side chain of Ser 365, indicating very strong affinity to the hAHR binding pocket. Due to symmetry of the

TCDD scaffold and possibility of establishing a second HB with the side chain of His 291 at the opposite side of Ser 365 in the binding pocket, the tautomerization state His-E was also included in the model. Based on His 291-E, TCDD docked with a score of -26.38 and established a HB with both side chains of His 291 and Ser 365 (Table 2, Fig. 1A). CH223191 docked with a score of -13.99 also involving the side chain of Ser 365 (Table 2, Fig. 1B), indicating favorable docking with the hAHR binding pocket. All three mITP congeners docked to hAHR in the presence of both His 291 tautomerization states with the same HB pattern involving the side chain of Cys 333 and Ser 365. The highest favorable score was obtained for the *meta* and *para* congener (His-E, Table 2, Fig. 1C,D). The *ortho* congener docked but did not bind favorably to hAHR (Table 2).

TCDD and the mITP congeners were also docked within each zebrafish AHR isoform. In AHR2, the human residue Ser 365 is replaced by an alanine (Bisson *et al.*, 2009). TCDD docked similarly in both tautomerization states of His 296 docking with a score of -21.86 (His-E) and established a HB with the side chain of Gln 388 (Table 2, Fig. 1E). CH223191 docked with a score of -12.04 also interacting with the side chain of Gln 388 (Table 2, Fig. 1F). All three mITP congeners docked in the binding pocket of AHR2 in both tautomerization states of His 296. The *meta* congener produced the highest score of -10.67 (His-E), establishing a HB with the side chain of His 296 (Table 2, Fig. 1G). The *para* (Fig. 1H) and *ortho* congeners both docked but did not bind favorably (Table 2).

In AHR1B, the human residue Ser 365 is replaced by an alanine (Bisson *et al.* 2009). TCDD docked similarly in both tautomerization states of His 296 with a score of -17.48 (His-E, Table 2, Fig. 1I). CH223191 and the *meta*- and *para*-mITP congeners docked in the binding pocket in both tautomerization states of His 296. CH223191 docked with a score of -17.87 (Table 2, Fig. 1J), whereas the *meta*- and *para*-mITP congeners docked with scores of -13.08 and -9.51 in the His-E tautomerization state, respectively, establishing a double HB with the side chain of Asn 341 (Table 2, Fig. 1K,L). The *ortho* congener did not dock. In the AHR1A residue, Tyr 296 replaces His 296, which is conserved in AHR2 and AHR1B, but also in mouse and human AHR (Bisson *et al.* 2009; Goodale *et al.* 2012). This substitution, along with Ala386Thr and Gln388His, decreases the volume and changes the polarity of the AHR1A binding pocket and leads a differential ligand affinity relative to AHR2 and AHR1B (Bisson *et al.* 2009). In AHR1A, TCDD docked with score of -8.24 (Table 2). The *ortho*- and *para*-mITP congeners did not dock. CH223191 and the *meta* congener docked with an unfavorable score (Table 2), establishing an HB interaction with the side chain of Tyr 296. Overall, these data suggest that the *meta*- and *para*-mITP congeners possess favorable binding towards hAHR and zebrafish AHR2 and AHR1B, but not AHR1A.

3.2. AHR knockdown does not prevent mITP-induced cardiotoxicity

Similar to findings reported within McGee *et al.* (2013), we first confirmed that (1) mITP-induced cardiotoxicity is concentration-dependent (Fig. S1) and (2) CH223191 mitigates mITP-induced cardiotoxicity and CYP1A expression (Fig. S2). Therefore, in order to begin determining whether mITP interacts with one or more AHR isoforms, we injected 5D embryos with control MO (CoMO), and embryos from a functional AHR2 knockout line (*ahr2*[hu3335]) with either AHR1B MO or both AHR1A and AHR1B MOs. All groups were

then treated with either vehicle or 0.2 μM mITP. In 5D embryos injected with CoMO, 100% exhibited PE (Fig. 2B). Surprisingly, all mITP-exposed *ahr2*[hu3335] morphants also showed severe PE in the majority of embryos (Fig. 2A,B). In *ahr2*[hu3335] mutant larvae injected with either CoMO, AHR1B MO, or co-injected with both AHR1A and AHR1B MO, there was 100%, 76%, and 80% PE, respectively (Fig. 2A,B). In the AHR1B/*ahr2*[hu3335] morphants, there was a statistically significant decrease in PE relative to 5D or *ahr2*[hu3335] embryos injected with CoMO but no decrease relative to *ahr2*[hu3335] co-injected with both AHR1A and AHR1B MOs.

3.3. mITP-induced CYP1A expression is AHR2- and AHR1B-dependent

To begin studying which AHR isoforms are activated by mITP, we utilized IHC and real-time qPCR to measure CYP1A induction at 72 hpf in all AHR knockdown scenarios. First, IHC indicated that 5D embryos injected with CoMO and exposed to vehicle exhibited no detectable CYP1A protein induction, while mITP-exposed embryos showed strong CYP1A protein induction in the vasculature, heart, and liver (Fig. 3A). On the other hand, mITP-exposed *ahr2*[hu3335] mutants injected with CoMO, AHR1B MO, and co-injected with both AHR1A and AHR1B MOs exhibited no detectable CYP1A protein induction using IHC (Fig. 3A). Using real-time qPCR to measure CYP1A mRNA, we found that *ahr2*[hu3335] CoMO-injected mutants still had an 18-fold increase in CYP1A expression in mITP-exposed embryos relative to vehicle controls (Fig. 3B). In the presence of AHR1B knockdown, CYP1A induction returned to AHR1B/*ahr2*[hu3335] morphant vehicle control levels (Fig. 3B). In addition, triple knockdown of AHR2, AHR1A, and AHR1B isoforms showed no further reduction in CYP1A induction relative to vehicle control levels in the same group (Fig. 3B). Lastly, using qualitative PCR to measure *ahr1a* and *ahr1b* mRNA, we found that MO-injected embryos had an exon deleted or an intron inserted, respectively, which suggests each isoform was successfully knocked down (Fig. 4).

4. Discussion

Using *in silico* structural homology modeling, TCDD was predicted to dock to AHR2 and AHR1B LBDs, but not AHR1A – which has been shown previously both *in vivo* and *in vitro* (Andreasen *et al.*, 2002; Goodale *et al.*, 2012; Karchner *et al.*, 2005). Comparing only docking scores with TCDD within each AHR isoform model, we predicted that AHR2 and AHR1B – but not AHR1A – would bind both CH223191 and mITP (Table 2). As mITP is a mixture of *meta-*, *para-*, and *ortho-*substituted mITP congeners, we tested whether these three congeners may dock to hAHR and zebrafish AHR1A, AHR1B, and AHR2 *in silico*, and found that *meta-*mITP docked favorably to hAHR and zebrafish AHR2 and AHR1B, while *para-*mITP docked favorably to hAHR and zebrafish AHR1B. Previously, McGee *et al.* (2013) used an *in vitro* human AHR reporter assay and demonstrated that mITP exposure resulted in activation of hAHR-dependent transcription. However, because of the current lack of commercially available analytical standards for mITP congeners, we were unable to separate mITP into its individual congeners to test the hypothesis that *meta* and *para* – but not *ortho* – activates AHR2 and AHR1B isoforms as was predicted *in silico*. Moreover, it is important to note that the mITP sample used in this study is from one batch of FM550 and, as a result, the ratio of individual congeners may vary from batch to batch.

The AHR is known for its promiscuity and various functional activities, including crosstalk with other receptors and differential expression of AHR response elements with various exogenous ligands (Denison *et al.*, 2011). Therefore, understanding the role of the AHR in developmental toxicity can often be complicated. Utilizing CH223191 as a pharmacologic tool, we confirmed results seen in McGee *et al.* (2013) that suggested mITP- induced cardiotoxicity was AHR-dependent. However, using *ahr2*[hu3335] zebrafish along with AHR1A and AHR1B MOs, we were able to more clearly determine the role of the AHR in mITP-induced cardiotoxicity. In Goodale *et al.* (2012), *ahr2*[hu3335] zebrafish were successfully utilized to rescue severe TCDD-induced developmental toxicity normally observed in wild-type zebrafish at the same nominal concentrations. Also, for the first time, Goodale *et al.* (2012) knocked down all three zebrafish AHR isoforms and, as a result, rescued leflunomide-induced CYP1A expression that activated all three AHR isoforms. In a similar way, we were able to knockdown all three AHR isoforms to study the interaction between mITP and AHR and to determine whether this interaction results in cardiotoxicity in zebrafish. As a result, we found that mITP-induced CYP1A expression is certainly mediated through the AHR2 and AHR1B isoforms, but that cardiotoxicity is AHR-independent.

Real-time qPCR results showed that CYP1A mRNA expression returned to AHR1B/*ahr2*[hu3335] morphant vehicle control levels upon AHR2 and AHR1B knockdown and that knockdown of all three AHR isoforms together did not further affect CYP1A expression. In addition, IHC results showed that 5D zebrafish had strong CYP1A protein induction indicative of AHR2 activation (Goodale *et al.* 2012), while *ahr2*[hu3335] zebrafish did not have any detectable CYP1A protein induction. These data suggest, as was predicted *in silico*, that mITP does activate AHR2 and AHR1B and does not activate AHR1A. Though PE prevalence decreased upon AHR1B knockdown in *ahr2*[hu3335] zebrafish, and by itself may suggest that AHR1B has a role in mediating cardiotoxicity, PE prevalence increased upon knockdown of all three AHR isoforms. Furthermore, *ahr2*[hu3335] control groups exhibited varying background PE that could explain the difference in the AHR1B/*ahr2*[hu3335] group. It is also conceivable that AHR1A knockdown exacerbates mITP-induced cardiotoxicity, as previously shown with PCB126 and some PAHs (Garner *et al.*, 2013); however, since CYP1A expression was not affected, this scenario is unlikely. Taken together, these data suggest that CH223191 antagonizes another target in addition to AHR that results in the protection from the induction of cardiotoxicity.

CH223191 has been previously used in combination with TCDD both *in vitro* and *in vivo* to investigate the role of AHR in mammalian reproduction, human glioma development, and acetylcholinesterase regulation (Brembilla *et al.*, 2011; Petroff *et al.*, 2011; Xie *et al.*, 2013). First identified through a chemical library screen (Kim *et al.*, 2006), CH223191 has also been used as a pharmacologic tool to study the toxicity of and AHR interactions with androgenic anabolic steroids, certain PAHs, and most recently mITP and TPP (Gramatzki *et al.*, 2009; McGee *et al.*, 2013; Moon *et al.*, 2012). However, CH223191 alone has been shown to cause AHR-independent cell proliferation in both human and murine hepatoma cell lines (Choi *et al.*, 2012). Moreover, CH223191 antagonism is ligand-dependent as it does not antagonize certain PAHs, flavonoids and indirubin, including benzo(a)anthracene,

benzo(k)fluoranthene, and β-Naphthoflavone (Zhao *et al.*, 2010). Using *in silico* structural homology modeling we predicted that CH223191 docks in AHR2 and AHR1B LBDs and we showed that CH223191 treatment results in reduced CYP1A expression relative to vehicle controls (Fig. S2). It remains a possibility that CH223191 may induce other AHR-dependent genes. Lastly, we suggest that CH223191 may antagonize a pathway other than AHR. Overall, these discoveries indicate that CH223191 alone is not sufficient to determine AHR-dependent toxicity.

McGee *et al.* (2013) showed that TPP – another major APE component of FM550 – exhibits a similar cardiotoxic phenotype as mITP, resulting in severe PE and abnormal cardiac looping. However, in the same study, TPP did not activate hAHR, did not induce CYP1A expression, and the observed cardiotoxicity was not rescued by CH223191. Nevertheless, due to structural similarities of mITP and TPP (the former only being different from a substitution of an isopropyl group on one of the three benzene rings), these two compounds (or a common metabolite) may cause cardiotoxicity via the same pathway. Although the metabolites of mITP are currently unknown, many Phase-I metabolites of TPP have been identified, including the metabolite diphenyl phosphate (DPP) resulting from O-dealkylation, as well as metabolites resulting from di-hydroxylation and both hydroxylation and O-dealkylation (Sasaki *et al.*, 1984; Van den Eede *et al.*, 2013). It is possible that mITP has similar metabolites as TPP, namely DPP and the metabolite resulting from hydroxylation and O-dealkylation. If this is the case, metabolites of mITP and TPP may cause AHR-independent cardiotoxicity in developing zebrafish. On the other hand, the CH223191 rescue of cardiotoxicity caused by mITP and not TPP may be a function of how CH223191 targets and possibly antagonizes other pathways. For instance, CH223191 may exhibit ligand-dependent antagonism with mITP and not TPP through an AHR-independent pathway, or may be a selective receptor modulator or allosteric regulator that results in exclusion of mITP and not TPP from a specific receptor-binding site (Choi *et al.*, 2012).

Though the mechanism of mITP- and TPP-induced developmental toxicity is not yet understood, it is possible that the PE and tube-heart phenotypes have similar pathological mechanisms. Previous studies have demonstrated that TPP causes upregulation in certain peroxisome proliferator-activated receptor α- and thyroid hormone receptor α-dependent genes (Liu *et al.* 2013). In human preparations, TPP has also been demonstrated to cause endocrine disrupting effects by acting as an estrogen receptor α and β agonist and androgen receptor antagonist (Kojima *et al.*, 2013). Further studies should be conducted to determine whether mITP and TPP have common metabolites and receptor targets, and whether these two chemicals induce expression of similar gene networks. In addition, a recent study demonstrated that constituents from crude oil (PAHs) can interfere with the excitation-contraction coupling of cardiomyocytes isolated from bluefin and yellowfin tunas (Brette *et al.*, 2014). Specifically, the disruption of cardiomyocyte repolarization is caused by direct blocking of potassium ion channels and decreased calcium current and calcium cycling. This mechanism is proposed to explain some elements of cardiotoxicity in developing fish, including cardiac arrhythmia, PE and overall cardiac failure (Brette *et al.* 2014). However, it is currently unknown whether the vast number of compounds that induce these phenotypes cause developmental toxicity through a common mechanism (Truong *et al.* 2013).

In summary, the findings in the present study show that additional research is needed to elucidate the developmental toxicity of mITP and FM550 more broadly. Previously, because of pconcerns about brominated FRs, the halogenated components of FM550 were investigated first. Specifically, TBPH has been shown to cause thyroid, liver, and testis toxicity in developing rodents, and TBB and TBPH have both been demonstrated to be endocrine disruptors at environmentally relevant levels (Springer *et al.*, 2012; Patisaul *et al.*, 2013). The present study is only the second to look specifically at the potential health effects from mITP. Though we showed mITP is an AHR agonist that causes AHR-independent cardiotoxicity in zebrafish, little is known regarding the downstream mechanisms. Given the widespread use of mITP and other APEs (particularly TPP), a more thorough evaluation of mITP should be undertaken in order to determine the potential human health and ecological risks.

Supplementary Material

Refer to Web version on PubMed Central for supplementary material.

Acknowledgments

References

Abagyan R, Totrov M, Kuznetsov D. ICM—A new method for protein modeling and design: Applications to docking and structure prediction from the distorted native conformation. J Comput Chem. 1994; 15(5):488–506.

Andreasen EA, Hahn ME, Heideman W, Peterson RE, Tanguay RL. The zebrafish (Danio rerio) aryl hydrocarbon receptor type 1 is a novel vertebrate receptor. Mol Pharmacol. 2002; 62:234–249. [PubMed: 12130674]

Bisson WH, Koch DC, O'Donnell EF, Khalil SM, Kerkvliet NI, Tanguay RL, Abagyan R, Kolluri SK. Modeling of the arylhydrocarbon receptor (AhR) ligand binding domain and its utility in virtual ligand screening to predict new AhR ligands. Journal of Medicinal Chemistry. 2009; 52:5635–5641. [PubMed: 19719119]

Brembilla NC, Ramirez JM, Chicheportiche R, Sorg O, Saurat JH, Chizzolini C. In vivo dioxin favors interleukin-22 production by human CD4+ T cells in an aryl hydrocarbon receptor (AhR)-dependent manner. PloS one. 2011; 6(4):e18741. [PubMed: 21525997]

Brette F, Machado B, Cros C, Incardona JP, Scholz NL, Block BA. Crude oil impairs cardiac excitation-contraction coupling in fish. Science (New York, NY). 2014; 343(6172):772–6.

Choi EY, Lee H, Dingle RWC, Kim KB, Swanson HI. Development of novel CH223191-based antagonists of the aryl hydrocarbon receptor. Molecular Pharmacology. 2012; 81(1):3–11. [PubMed: 21967751]

Costa LG, Giordano G. Developmental neurotoxicity of polybrominated diphenyl ether (PBDE) flame retardants. Neurotoxicology. 2007; 28(6):1047–1067. [PubMed: 17904639]

Davis EF, Klosterhaus SL, Stapleton HM. Measurement of flame retardants and triclosan in municipal sewage sludge and biosolids. Environment International. 2012; 40:1–7. [PubMed: 22280921]

Denison MS, Nagy SR. Activation of the aryl hydrocarbon receptor by structurally diverse exogenous and endogenous chemicals. Annual Review of Pharmacology and Toxicology. 2003; 43:309–34.

Garner LVT, Brown DR, Di Giulio RT. Knockdown of AHR1A but not AHR1B exacerbates PAH and PCB-126 toxicity in zebrafish (Danio rerio) embryos. Aquatic Toxicology. 2013; 142-143C:336–346. [PubMed: 24084256]

Goodale BC, La Du JK, Bisson WH, Janszen DB, Waters KM, Tanguay RL. AHR2 mutant reveals functional diversity of aryl hydrocarbon receptors in zebrafish. PloS one. 2012; 7(1):e29346. [PubMed: 22242167]

Gramatzki D, Pantazis G, Schittenhelm J, Tabatabai G, Köhle C, Wick W, Schwarz M, Weller M, Tritschler I. Aryl hydrocarbon receptor inhibition downregulates the TGF-beta/Smad pathway in human glioblastoma cells. Oncogene. 2009; 28(28):2593–605. [PubMed: 19465936]

Herbstman JB, Sjodin A, Kurzon M, Lederman SA, Jones RS, Rauh V, Needleman LL, Tang D, Niedzwiecki M, Wang RY, Perera F. Prenatal exposure to PBDEs and neurodevelopment. Environ Health Perspect. 2010; 118(5):712–719. [PubMed: 20056561]

Incardona JP, Day HL, Collier TK, Scholz NL. Developmental toxicity of 4-ring polycyclic aromatic hydrocarbons in zebrafish is differentially dependent on AH receptor isoforms and hepatic cytochrome P4501A metabolism. Toxicology and Applied Pharmacology. 2006; 217(3):308–21. [PubMed: 17112560]

Incardona JP, Linbo TL, Scholz NL. Cardiac toxicity of 5-ring polycyclic aromatic hydrocarbons is differentially dependent on the aryl hydrocarbon receptor 2 isoform during zebrafish development. Toxicology and Applied Pharmacology. 2011; 257(2):242–9. [PubMed: 21964300]

Jönsson ME, Kubota A, Timme-Laragy AR, Woodin B, Stegeman JJ. AHR2-dependence of PCB126 effects on the swim bladder in relation to expression of CYP1 and cox-2 genes in developing zebrafish. Toxicology and Applied Pharmacology. 2012; 265(2):166–74. [PubMed: 23036320]

Karchner SI, Franks DG, Hahn ME. AHR1B, a new functional aryl hydrocarbon receptor in zebrafish: tandem arrangement of ahr1b and ahr2 genes. The Biochemical Journal. 2005; 392(1):153–61. [PubMed: 16042621]

Katritch V, Rueda M, Abagyan R. Ligand-guided receptor optimization. Methods in Molecular Biology. 2012; 857:189–205. [PubMed: 22323222]

Kim SH, Henry EC, Kim DK, Kim YH, Shin KJ, Han MS, Lee TG, Kang JK, Gasiewicz TA, Ryu SH, Suh PG. Novel compound 2-methyl-2H-pyrazole-3-carboxylic acid (2-methyl-4-o-tolylazo-phenyl)- amide (CH-223191) prevents 2,3,7,8-TCDD-induced toxicity by antagonizing the aryl hydrocarbon receptor. Mol Pharmacol. 2006; 69:1871–1878. [PubMed: 16540597]

Kojima H, Takeuchia S, Itohb T, Iidac M, Kobayashis S, Yoshidab T. In vitro endocrine disruption potential of organophosphate flame retardants via human nuclear receptors. Toxicology. 2013; 314(1):76–83. [PubMed: 24051214]

Lam JCW, Lau RKF, Murphy MB, Lam PKS. Temporal trends of hexabromocyclododecanes (HBCDs) and polybrominated diphenyl ethers (PBDEs) and detection of two novel flame retardants in marine mammals from Hong Kong, South China. Environmental Science and Technology. 2009; 43(18):6944–9. [PubMed: 19806725]

Liu C, Wang Q, Liang K, Liu J, Zhou B, Zhang X, Liu H, Giesy JP, Yu H. Effects of tris(1,3-dichloro-2-propyl) phosphate and triphenyl phosphate on receptor-associated mRNA expression in zebrafish embryos/larvae. Aquatic Toxicology. 2013; 128-129:147–157. [PubMed: 23306105]

Ma Y, Venier M, Hites RA. 2-Ethylhexyl Tetrabromobenzoate and Bis (2-ethylhexyl) Tetrabromophthalate Flame Retardants in the Great Lakes Atmosphere. Environmental Science and Technology. 2012; 46:204–208. [PubMed: 22128844]

McGee SP, Konstantinov A, Stapleton HM, Volz DC. Aryl phosphate esters within a major PentaBDE replacement product induce cardiotoxicity in developing zebrafish embryos: potential role of the aryl hydrocarbon receptor. Toxicol Sci. 2013; 133(1):144–156. [PubMed: 23377616]

Meeker JD, Stapleton HM. House dust concentrations of organophosphate flame retardants in relation to hormone levels and semen quality parameters. Environmental Health Perspectives. 2010; 118(3):318–23. [PubMed: 20194068]

Moon HY, Kim SH, Ryu SH, Suh PG. The androgenic anabolic steroid tetrahydrogestrinone produces dioxin-like effects via the aryl hydrocarbon receptor. Toxicology In Vitro. 2012; 26(7):1129–33. [PubMed: 22664790]

Patisaul HB, Roberts SC, Mabrey N, McCaffrey KA, Gear RB, Braun J, Belcher SM, Stapleton HM. Accumulation and endocrine disrupting effects of the flame retardant Mixture Firemaster 550 in rats: An exploratory assessment. Journal of Biochemical and Molecular Toxicology. 2012; 27(2): 124–136. [PubMed: 23139171]

Petroff BK, Valdez KE, Brown SB, Piasecka J, Albertini DF. The aryl hydrocarbon receptor agonist 2,3,7,8-tetrachloro-dibenzo-p-dioxin (TCDD) alters early embryonic development in a rat IVF exposure model. Reproductive Toxicology. 2011; 32(3):286–92. [PubMed: 21835239]

Prasch AL, Teraoka H, Carney SA, Dong W, Hiraga T, Stegeman JJ, Heideman W, Peterson RE. Aryl hydrocarbon receptor 2 mediates 2,3,7,8-tetrachlorodibenzo-p-dioxin developmental toxicity in zebrafish. Toxicol Sci. 2003; 76:138–150. [PubMed: 12883077]

Rahman F, Langford KH, Scrimshaw MD, Lester JN. Polybrominated diphenyl ether (PBDE) flame retardants. Sci Total Environ. 2001; 275(1-3):1–17. [PubMed: 11482396]

Reimers MJ, La Du JK, Periera CB, Giovanini J, Tanguay RL. Ethanol-dependent toxicity in zebrafish is partially attenuated by antioxidants. Neurotoxicology and Teratology. 2006; 28(4):497–508. [PubMed: 16904866]

Sasaki K, Suzuki T, Takeda M, Uchiyama M. Metabolism of phosphoric-acid triesters by rat-liver homogenate. Bulletin of Environmental Contamination and Toxicology. 1984; 33(3):281–288. [PubMed: 6478075]

Springer C, Dere E, Hall SJ, Mcdonnell EV, Roberts SC, Butt CM, Stapleton HM, Watkins DJ, McClean MD, Webster TF, Schlezinger JJ, Boekelheide K. Rodent Thyroid, Liver, and Fetal Testis Toxicity of the Monoester Metabolite of Bis-(2-ethylhexyl) Tetrabromophthalate (TBPH), a Novel Brominated Flame Retardant Present in Indoor Dust. Environmental Health Perspectives. 2012; 120(12):1711–1720. [PubMed: 23014847]

Stapleton HM, Allen JG, Kelly SM, Konstantinov A, Klosterhaus S, Watkins D, McClean MD, Webster TF. Alternate and new brominated flame retardants detected in U.S. house dust. Environ Sci Technol. 2008; 42(18):6910–6916. [PubMed: 18853808]

Stapleton HM, Klosterhaus S, Eagle S, Fuh J, Meeker JD, Blum A, Webster TF. Detection of organophosphate flame retardants in furniture foam and U.S. house dust. Environ Sci Technol. 2009; 43(19):7490–7495. [PubMed: 19848166]

Tanguay RL, Abnet CC, Heideman W, Peterson RE. Cloning and characterization of the zebrafish (Danio rerio) aryl hydrocarbon receptor. Biochmica et Biophysica Acta. 1999; 1444(1):35–48.

Totrov, M.; Abagyan, R. Protein-ligand docking as an energy optimization problem. In: Raffa, RB., editor. Drug-receptor thermodynamics: introduction and experimental application. John Wiley and Sons; New York: 2001. p. 603-624.

Truong L, Reif DM, St Mary L, Geier MC, Truong HD, Tanguay RL. Multidimensional in vivo hazard assessment using zebrafish. Toxicological Sciences. 2014; 137(1):212–33. [PubMed: 24136191]

Tullo A. Great Lakes to phase out two flame-retardants. Chemical and Engineering News. 2003; 81(45):13.

Van den Eede N, Maho W, Erratico C, Neels H, Covaci A. First insights in the metabolism of phosphate flame retardants and plasticizers using human liver fractions. Toxicology Letters. 2013; 223(1):9–15. [PubMed: 23994729]

Xie HQ, Xu HM, Fu HL, Hu Q, Tian WJ, Pei XH, Zhao B. AhR-Mediated Effects of Dioxin on Neuronal Acetylcholinesterase Expression in Vitro. Environmental Health Perspectives. 2013; 121(5):613–8. [PubMed: 23426015]

Zhao B, Degroot DE, Hayashi A, He G, Denison MS. CH223191 is a ligand-selective antagonist of the Ah (Dioxin) receptor. Toxicological Sciences. 2010; 117(2):393–403. [PubMed: 20634293]

## Abbreviations used

AHR	aryl hydrocarbon receptor
CYP1A	cytochrome P450 1A
FM550	Firemaster 550

|	
IHC	immunohistochemistry
LBD	ligand-binding domain
mITP	mono-substituted isopropylated triaryl phosphate
MO	morpholino
PAH	polycyclic aromatic hydrocarbon
qPCR	quantitative polymerase chain reaction
PE	pericardial edema
TCDD	2,3,7,8-tetrachlorodibenzo-p-dioxin
TPP	triphenyl phosphate

Highlights

- Mono-substituted isopropylated triaryl phosphate causes AHR-independent toxicity

- mITP activates AHR2 and AHR1B isoforms in zebrafish

- *In silico* AHR homology modeling correctly predicted AHR-isoform dependence

- mITP causes toxicity through an unknown pathway also antagonized by the AHR antagonist CH223191
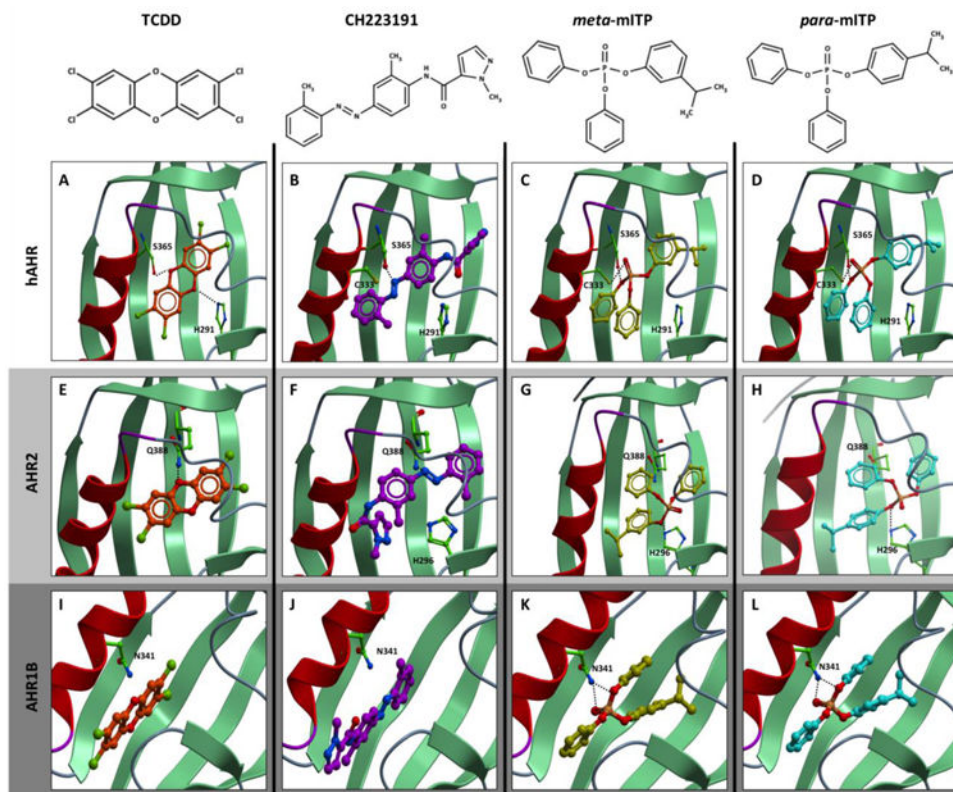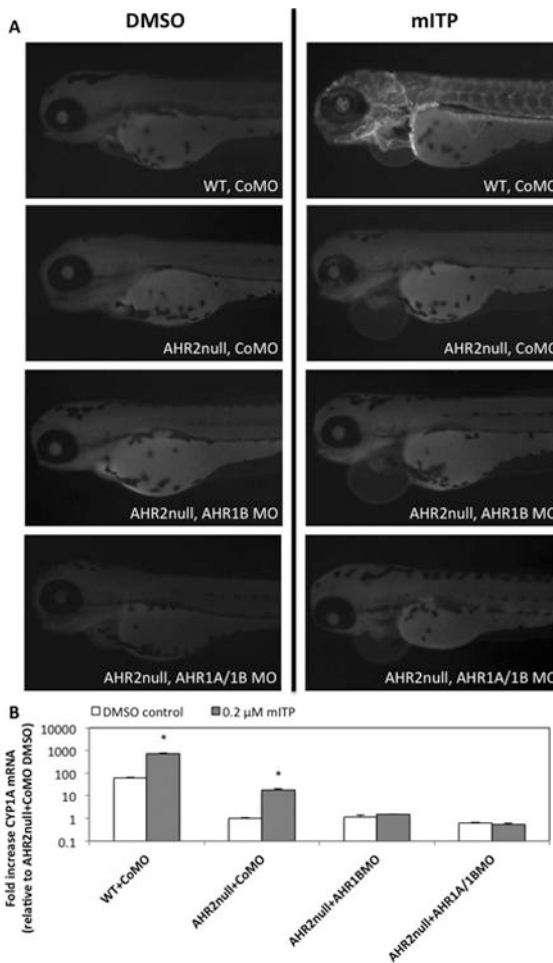
Figure 1.
Docking of TCDD, CH223191 and meta- and para-mITP congeners in human and zebrafish AHR2 and AHR1B LBDs (Molsoft ICM). ortho-mITP was predicted to dock in AHR2, but with an unfavorable score (not shown). Docked ligands are displayed as sticks and colored by atom type, with carbon atoms in orange (TCDD), purple (CH223191), yellow (meta-mITP) and cyan (para-mITP). Protein residues are displayed as stick with the carbon atoms colored in green. Secondary structure is displayed as ribbon. Protein-ligand HB interactions are displayed as dashed black lines.
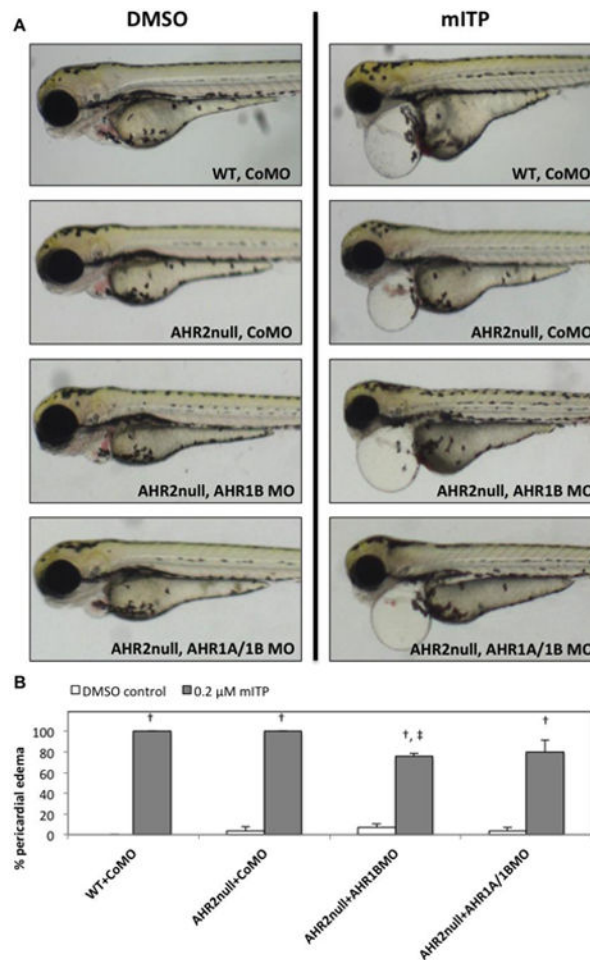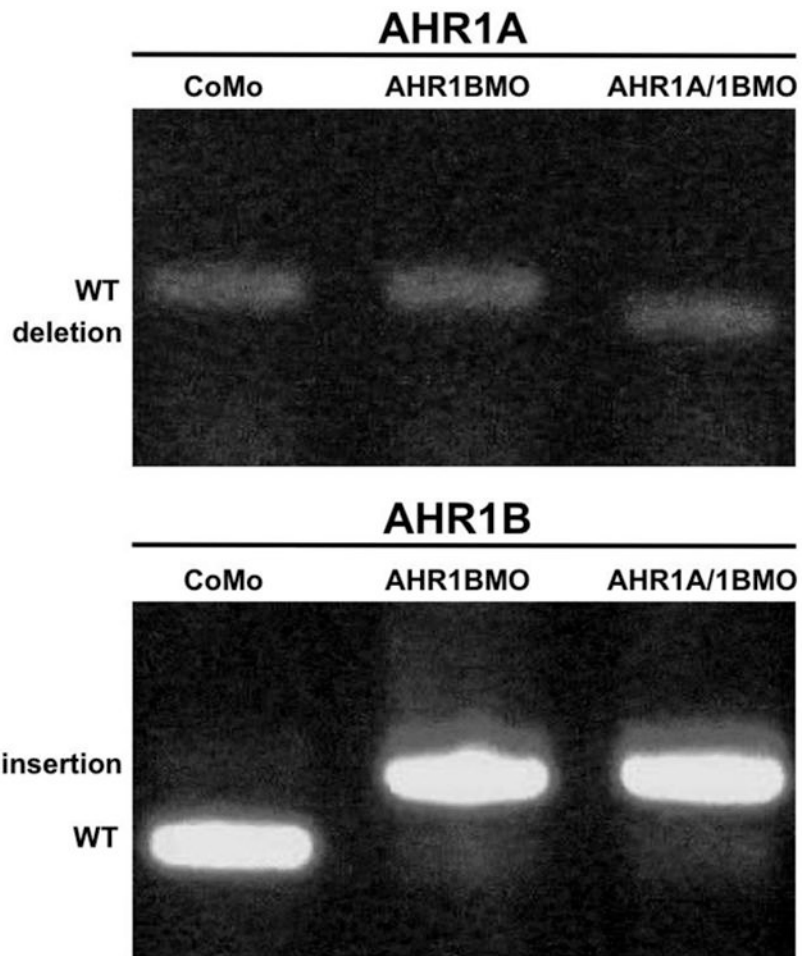
Figure 2.
mITP-induced cardiotoxicity is AHR-independent. 5D embryos (WT) were injected with CoMO, and ahr2hu3335 mutant embryos (AHR2null) were injected with either CoMO, AHR1B MO, or co-injected with AHR1A and AHR1B MOs. (A) Representative bright-field images of WT and AHR2null morphants exposed to either vehicle control (0.1% DMSO) or 0.2 μM mITP. (B) Percent PE is mean ± SE. All groups were allowed to develop until 72 hpf. Dagger (†) denotes a statistically significant increase in PE in mITP-exposed embryos relative to vehicle controls within the same group ($p < 0.05$), whereas double dagger (‡) denotes a statistically significant decrease in PE relative to mITP-exposed CoMO-injected WT fish ($p < 0.05$). N = 3 replicate vials and 9 to 10 fish per replicate.

Figure 3.
CYP1A induction is AHR2 and AHR1B-dependent. (A) Representative fluorescent images at 72 hpf of CYP1A protein expression of CoMO-injected WT embryos, CoMO-injected AHR2null, AHR1B MO-injected AHR2null, and AHR2null co-injected with AHR1A and AHR1B MOs. All groups were exposed to either vehicle control (0.1% DMSO) or 0.2 μM mITP. (B) CYP1A mRNA induction normalized to β-actin (internal control) at 72 hpf. All groups were exposed to either vehicle control (0.1% DMSO) or 0.2 μM mITP. Fold increase is mean ± SE. N = 3 replicate vials each with 9 to 10 fish per replicate. Asterisk (*) denotes a statistically significant increase in treatment groups relative to vehicle controls within the same group ($p < 0.05$).

Figure 4.
AHR1A and AHR1B MOs caused mis-splice in target mRNA. AHR1A and AHR1B fragments spanning the MO target sites were amplified using PCR. cDNA was from the same 72-hpf embryos that were used for CYP1A qPCR.

Table 1

Primer sequences for PCR.

Target	Forward Primer (5′ – 3′)	Reverse Primer (5′ – 3′)
cyp1a	TGCCGATTTCATCCCTTTCC	AGAGCCGTGCTGATAGTGTC
ahr1a	CGCAAAAGGAGGAAACCTGTC	CCTGTAGCAAAAATTCCCCCT
ahr1b	CTTTGTGTGTCGTTTCCGATGCC	GCACAGTAGAGCATATCAGCTGC
β-actin	AAGCAGGAGTACGATGAGTC	TGGAGTCCTCAGATGCATTG

Table 2

Predicted binding scores for human AHR and zebrafish AHR2, AHR1B, and AHR1A isoforms.

	hAHR	AHR2	AHR1B	AHR1A
TCDD	-26.38	-21.86	-17.48	-8.24
CH223191	-13.99	-12.04	-17.87	+
ortho-**mITP**	+	-0.96	nd	nd
meta-**mITP**	-16.89	-10.67	-13.08	+
para-**mITP**	-14.63	+	-9.51	nd

h, human; nd, not docked; +, docked with a positive score